Blockage and Directivity in 60 GHz Wireless Personal Area Networks: From Cross-Layer Model to Multihop MAC Design

Sumit Singh, *Student Member, IEEE,* Federico Ziliotto, Upamanyu Madhow, *Fellow, IEEE,* Elizabeth M. Belding, *Senior Member, IEEE,* and Mark Rodwell, *Fellow, IEEE*

***Abstract*—We present a cross-layer modeling and design approach for multiGigabit indoor wireless personal area networks (WPANs) utilizing the unlicensed millimeter (mm) wave spectrum in the 60 GHz band. Our approach accounts for the following two characteristics that sharply distinguish mm wave networking from that at lower carrier frequencies. First, mm wave links are inherently directional: directivity is required to overcome the higher path loss at smaller wavelengths, and it is feasible with compact, low-cost circuit board antenna arrays. Second, indoor mm wave links are highly susceptible to blockage because of the limited ability to diffract around obstacles such as the human body and furniture. We develop a diffraction-based model to determine network link connectivity as a function of the locations of stationary and moving obstacles. For a centralized WPAN controlled by an access point, it is shown that multihop communication, with the introduction of a small number of relay nodes, is effective in maintaining network connectivity in scenarios where single-hop communication would suffer unacceptable outages. The proposed multihop MAC protocol accounts for the fact that every link in the WPAN is highly directional, and is shown, using packet level simulations, to maintain high network utilization with low overhead.**

***Index Terms*—Wireless personal area networks (WPAN), Millimeter wave WPANs, Millimeter wave propagation, 60 GHz networks, Medium Access Control (MAC).**

I. Introduction

We investigate indoor wireless personal area networks (WPANs) utilizing the 60 GHz "millimeter (mm) wave" band. With 7 GHz of unlicensed spectrum in the United States, and 3 GHz of unlicensed bandwidth in common with Europe and Japan, this band can potentially enable multiGigabit wireless communication products and applications standardized worldwide. Advances in the speeds of silicon semiconductor processes imply that mm wave radio frequency (RF) integrated circuits (ICs) are now feasible in CMOS, paving the way for economies of scale similar to those that have driven the growth of cellular and WiFi networks at lower carrier frequencies. Applications that could utilize the increased speeds enabled by 60 GHz WPANs include high-speed data transfer (e.g., of multimedia content) between devices such as cameras, camcorders, personal computers and televisions, as well as real-time streaming of both compressed and uncompressed high definition television (HDTV). This convergence of these hardware and application trends has fueled intense efforts in both research and standardization for mm wave communication [1]–[9]. However, the eventual success of these efforts depends on system designs that account for the fundamental differences between mm wave communication and existing wireless networks at lower carrier frequencies (e.g., from 900 MHz to 5 GHz). In particular, the goal of this paper is to introduce a cross-layer modeling and design approach that addresses two unique features of mm wave links: their vulnerability to blockage and their inherent directivity.

Blockage: Electromagnetic waves have very limited ability to diffract around obstacles whose size is significantly larger than the wavelength. Since the wavelength at 60 GHz is so small (5 mm), links are effectively blocked by obstacles such as humans and furniture. For example, blockage by a human can penalize the link budget by 20-30 dB. Human movement in a room, therefore, can cause intermittent blockage of mm wave WPAN links, resulting in a time-varying network topology. Maintaining seamless network connectivity and providing the QoS needed for applications such as HDTV in such a setting is a challenge for network protocol design which is fundamentally different from that at lower carrier frequencies. Meeting this challenge requires models that take into account diffraction (or the lack thereof), both for obtaining design insight and for performance evaluation.

Directivity: Millimeter wave links are inherently directional. The free space propagation loss between isotropic antennas scales as λ^2, where λ is the carrier wavelength, so that 60 GHz is 21.6 dB *worse* than 5 GHz for omnidirectional communication. On the other hand, for a fixed antenna aperture area (which depends on the transceiver form factor), directivity scales as $1/\lambda^2$, giving a gain of $1/\lambda^4$ when we account for both transmit and receive antennas. This corresponds to an overall scaling of $1/\lambda^2$, so that a 60 GHz link with directional transmission and reception can now become 21.6 dB *better* than a 5 GHz link, assuming nodes of similar form factor. In particular, steerable antenna arrays implemented as patterns of metal on circuit board can be employed to synthesize highly directional beams for 60 GHz nodes that are smaller than a typical WiFi access point. It is crucial to take advantage of this, given the difficulty of producing a large amount of

S. Singh, U. Madhow, and M. Rodwell are with the Department of Electrical and Computer Engineering, University of California, Santa Barbara, CA 93106, USA (email: sumit@ece.ucsb.edu).

F. Ziliotto was with the Department of Electrical and Computer Engineering, University of California, Santa Barbara, CA 93106, USA. He is now with Cisco Systems, Brussels, Belgium.

E. Belding is with the Department of Computer Science, University of California, Santa Barbara, CA 93106, USA.

Manuscript received Sep. 30, 2008; revised May 27, 2009.

transmit power at mm wave frequencies using low-cost, low-power silicon implementations.

Our approach: We propose a cross-layer modeling framework and a multihop directional MAC architecture for robust, multi-Gigabit, in-room WPANs. Each node has an electronically steerable directional antenna, so that the transmitters and receivers can steer beams towards each other. The key idea is to handle blockages by going around obstacles, rather than burning through them. Blockages that result in a 20 dB power loss require a 100-fold reduction in data rate in order to maintain the same reliability, when operating in a power-limited regime. On the other hand, routing around the obstacle by replacing the blocked link by 2 links only reduces throughput by a factor of two. We consider directional, line of sight (LOS) links, with each link operating at a fixed nominal data rate (e.g., 2 Gbps) when the LOS path is available. When the LOS path between two nodes is blocked, we route around it, still using directional LOS links. Assuming that there are enough spatially dispersed nodes, this multihop architecture provides both high power efficiency and robust connectivity in the face of stationary and moving obstacles typical of living room and office settings. In principle, it is also possible to use reflections from walls and other surfaces to steer around obstacles; however, not only do reflections result in a loss of link budget, but the efficacy of using them to avoid blockage is a sensitive function of node placement and the propagation environment. We therefore focus on whether it is possible to obtain robust network connectivity and high throughput with LOS links alone, using a small number of relays if necessary.

We consider the specific in-room scenario of several wireless terminals (WTs) controlled by a single access point (AP), with nominal operation consisting of direct, contention-free communication between the AP and each WT. When an AP discovers that its link to a WT is blocked, it sets up an alternate route based on its current topology information (the topology of the directional links is discovered during set-up, and regular opportunities for topology update are a part of the proposed MAC protocol). Due to the slow time scale of human movements (which are typically the cause of network topology changes) relative to the topology updates enabled by the protocol, our simulations show that the alternate routes computed by the AP are invariably functional. Thus, while outage rates for a given link can be quite high (as high as 60%), intelligent multihop networking effectively removes outages in connectivity between the AP and the WTs. An important component of our work is the development of simple models for time-varying blockage in typical WPAN environments that enable performance evaluation of the preceding architecture.

Summary of contributions: Our contributions are summarized as follows:

1) We propose and investigate an in-room WPAN architecture that addresses both blockage and directivity, the fundamental features that distinguish mm wave networks from those at lower frequencies. In particular, the proposed directional MAC protocol is designed for a network in which every link is constrained to be directional, without fallback to an omnidirectional mode for coordination as in most prior work. The protocol includes procedures for topology discovery and updates, and recovery from LOS link outages via multihop relay to the blocked nodes.

2) We analyze the effect of obstacles on the received signal strength via a site-specific mm wave propagation model based on the Fresnel-Kirchhoff diffraction theory. This provides a simple model to track the time evolution of link losses using deterministic computations, and hence the network connectivity for a given set of stationary and mobile obstacles whose geometry models a human.

3) We evaluate the performance of our multihop relay directional MAC protocol via analysis and extensive packet level simulations. The simulations verify the efficacy of multihop relay in maintaining consistently high throughput with low control overhead, despite frequent LOS link outages due to time-varying blockage.

Related work: To the best of our knowledge, there is no prior work on the design of mm wave WPANs with exclusively directional links in the literature, except for a conference publication with our own preliminary results [10]. There are many ongoing industry-led efforts aimed towards the standardization of 60 GHz WPAN network interfaces; for example, the IEEE 802.15 WPAN Millimeter Wave Alternative PHY Task Group 3c [7], the WirelessHD Consortium [8], and ECMA International [9]. The ECMA-387 specification for the 60 GHz WPAN PHY/MAC released in December 2008 also includes a relay mechanism to counter link blockage thereby affirming the timeliness of this work and the need for further research to better understand the efficacy of such mechanisms.

The use of directional antennas has been extensively studied for wireless networks operating in the lower frequency bands such as cellular and broadband networks, and over the last decade, on WiFi-based multihop networks [11]–[17]. In this context, the performance benefits of directional communication such as improved spatial reuse and extended directional communication range have an associated cost, because a number of problems arise due to, or are aggravated by, directional communication, such as the hidden terminal problem, deafness [16], and the problem of neighbor discovery. The typical solution in the literature is to employ a combination of directional and omnidirectional communication for critical control message exchanges (e.g., the four way handshake in IEEE 802.11) for medium access control. Such a dual-mode operation is not appropriate for the mm-wave WPANs that we envision, for which directionality is required at both the transmitter and the receiver simply to achieve reliable high data rate communication. For such networks, network protocols based on a directional mode alone (with the ability to choose the direction, either via sectorization or beamsteering) need to be developed. References [17], [18] propose fully-directional MAC protocols for multihop wireless networks: [17] proposes a directional slotted ALOHA protocol that exploits the adaptive beamforming capabilities of smart antenna arrays, whereas [18] presents a polling-based decentralized MAC protocol. However, none of the papers in the literature model or address the problem of frequent link outages due to blockage, which fundamentally alters the design tradeoffs for mm wave networks relative to those at lower carrier frequencies. In particular, far more agility needs

to be designed into the network protocols to handle the time-varying network topology with low overhead, while satisfying the stringent QoS requirements for the bandwidth-hungry applications driving the development of mm wave WPANs.

Network design efforts such as ours are motivated by recent advances in mm wave circuit design [1], [2], [4], including multiGigabit electronically steerable directional links [19], that indicate that low-cost commercially feasible realizations are within reach. In terms of the channel model we use, while our diffraction model is based on fundamental physics, we are motivated by the extensive body of knowledge on mm wave propagation measurement and modeling. Measurement campaigns in indoor environments include [20]–[29]. For typical indoor environments with omnidirectional antennas, specular reflections from surfaces are dominant contributors to the received signal power as compared with diffraction or scattering [24], [30]–[32]. Since the path that is the strongest in such a setting is the LOS path (if it is not blocked), this motivates restriction to LOS for maximizing power efficiency. The reduction of multipath for directional mm wave links [23], [32], [33] means that link budget calculations for a simple additive white Gaussian noise channel model are reasonably accurate for a directional LOS link. The susceptibility of mm wave links to blockage due to their weak diffraction characteristics is well known [23], [34], and the effect of human movement is investigated in [35], [36], but their impact on the network performance has not been studied previously. Many deterministic and statistical mm wave propagation models have been proposed based on channel measurement studies [25], [30], [37], but many of these focus on omnidirectional transmission (and possibly directional reception). Reference [38] provides line of sight (LOS)/ non-line of sight (NLOS) channel models developed by the IEEE 802.15 TG3c group for indoor WPAN environments. These statistical channel models do not account for the effect of moving obstacles such as humans on the network connectivity over time (e.g., deep fades for seconds), and are basically meant to be used for a comparison between different physical layer designs.

Outline: We describe our physical layer model in Section II, include a model for blockage by both stationary and moving obstacles. Simulation results with this model are used to motivate the need for multihop communication to provide robust network connectivity. Section III presents a multihop directional MAC for achieving such robustness, and estimates achievable rates accounting for overhead. In Section IV, packet-level simulations of MAC performance, taking into account the blockage model developed in Section II, are used to demonstrate the efficacy of our multihop architecture. Section V contains our conclusions, including a brief discussion of important areas for future research.

II. Physical Layer Model

We first describe an example link budget for a LOS 60 GHz link to give a feel for the required transmit signal power levels for the feasibility of WPANs with directional LOS links. However, we then abstract away from detailed design choices in the physical layer to focus on the key bottleneck for mm wave communication: blockage by obstacles. We describe in detail the calculations needed to compute diffraction-based path loss for a given obstacle configuration, and use the model to obtain the time-varying network connectivity. We show that, while any given link can frequently be in outage due to blockage, multihop communication can indeed provide robust connectivity. This motivates the multihop MAC in the next section.

Example Link Budget: We present simple calculations that indicate the feasibility of a plug-and-play WPAN. The directivity of an antenna is the ratio of the maximum power density (watts/m^2) to its average value over a sphere. The directivity of an antenna can be approximated as [39]:

$$D = \frac{40000}{\theta^o_{HP}\phi^o_{HP}}$$

where θ^o_{HP} and ϕ^o_{HP} are the horizontal and vertical beamwidths, respectively, of the antenna. For a WPAN application, we might design an antenna element to have a horizontal beamwidth of 120^o and a vertical beamwidth of 60^o, which allows a rough placement of nodes in order to ensure LOS to one or two neighbors. The directivity for such an element, which can be realized as a pattern of metal on circuit board, is 5.55 (or 7.4 dBi). If we put four such elements to form a steerable antenna array, we can get a directivity of 22 (or 13.4 dBi). Now, assuming an antenna directivity of 13.4 dBi at each end, we do a link budget for a QPSK system operating at 2 Gbps [40]. For a receiver noise figure of 6 dB, bit error rate of 10^{-9}, excess bandwidth of 50%, and assuming free space propagation, we obtain that the required transmit power for a nominal range of 10 meters is about 8 mW, including a 10 dB link margin. When split among four antenna elements, this transmit power corresponds to 2 mW of power per antenna element. RF front ends for obtaining these power levels are realizable with silicon semiconductor processes, thereby indicating the feasibility of low-cost, high-volume production of the kinds of WPAN nodes on which our architecture is based.

Adaptive Beamforming Antennas: We assume that all the WPAN nodes are equipped with electronically steerable antenna arrays that can be used to provide directivity on both transmit and receive. A receiving antenna array uses a training sequence in the PHY preamble of a packet to adjust the required array weights in order to adaptively beamform towards the direction of the signal of interest [41], using standard adaptive algorithms [42], such as least mean squares (LMS) or recursive least squares (RLS), or variants thereof. For a relatively small number of elements (e.g., 4-10), such algorithms converge quickly, so that packet-by-packet beamsteering with, say, 50 symbols training overhead, should be feasible. Thus, we assume that an idle node can quickly steer its receive antenna array towards an incoming signal: this amounts to "omnidirectional" sensing (restricted only by the field of view of the antennas in the array), but directional reception. The beamforming weights learnt when receiving from a given node can then be used to transmit back to that node, using channel reciprocity, so that transmission is directional as well. Alternatively, the transmitter or receiver could choose from among a fixed number of sectors, thus discretizing the beamforming function.

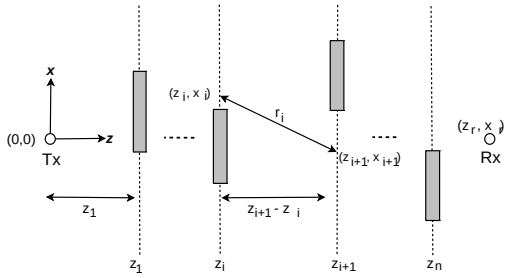

Fig. 1. Multiple obstacles scenario.

Diffraction due to obstacles: We use a simple geometric model to estimate the diffraction loss along the LOS path between two nodes, taking into account the node placements, the locations and dimensions of obstacles, and the room dimensions. We neglect the contribution from the reflected signals to the received signal power; narrow beam directional antennas along the LOS direction substantially reduce the contribution of reflected multipath components [23], [32], [33], [36].

We make the following simplifying assumptions in modeling obstacles:
1) The attenuation due to an obstacle in the LOS path is so high that the energy of the signal propagating through the obstacle is negligible. In other words, we only consider the obstacles that can cause a significant attenuation to a signal propagating through them. For mm waves, most of the common obstructions in indoor environments, such as human beings, thick walls and furniture, fall in this category. Thus, the link gain is only due to diffraction around the obstacle.
2) The human body is approximated as a perfect conducting cylinder, whose projection on the plane perpendicular to the line of sight is considered for diffraction calculations. Other obstacles are approximated in a similar manner.

Diffraction of electromagnetic waves [43], [44] can be intuitively explained in terms of a fundamental principle from physical optics: the Huygens' principle which states that "*each point on a primary wavefront can be considered to be a new source of a secondary spherical wave and that a secondary wavefront can be constructed as the envelope of these secondary spherical waves*" [44]. An obstacle blocks a subset of these secondary waves, and the field at a point of interest beyond the obstacle can be obtained by summing up the contributions from the remaining secondary waves. The mathematics of these computations is often referred to as Kirchhoff theory [43]. Diffraction theory has been widely used to study terrain diffraction in the context of wireless cellular systems primarily using the knife-edge diffraction model [45]–[49].

Fig. 1 shows the propagation path from a source Tx to a receiver Rx obstructed by n obstacles, modeled as perfect conducting strips. To begin with, assume the transmitter and the receiver to be isotropic point sources (we specify later how to incorporate directivity). We now calculate the diffracted electric field at the receiver by successively applying Huygens' principle at each obstacle along the LOS from the transmitter to the receiver. This is done by summing up contributions from "non-blocked" secondary sources at one obstacle, at the plane of the next obstacle. These iterative computations are initialized by specifying the electric field $E_1(x_1)$ at a point (z_1, x_1) on the plane containing obstacle 1:

$$E_1(x_1) = \frac{E_c}{r_1} e^{-j\beta r_1} \tag{1}$$

where E_c is a constant, $r_1 = \sqrt{z_1^2 + x_1^2}$ and $\beta = \frac{2\pi}{\lambda}$ is the phase constant for wavelength λ (the time variation $e^{-j\omega t}$ is suppressed).

We now compute the gain from the ith plane to the $(i+1)$th plane of interest, where $i = 1, ..., n-1$. The same computation applied for $i = n$ gives the field at the receiver, whose location corresponds to the $(n+1)$th plane. Let us now specify a typical step (say step i) in these calculations. The electric field $E_{i+1}(x)$ at a point (z_{i+1}, x_{i+1}) in the $(i+1)$th plane is calculated by superimposing the contributions from the Huygens' point sources at points (z', x') in the i^{th} window, as follows:

$$E_{i+1}(x) = \int_{-\infty}^{\infty} h_i(x') E_i(x') g_i(x - x') dx' \tag{2}$$

where function $h_i(x') = e^{-j\beta(z-z')} \sqrt{\frac{jz'}{\lambda z(z-z')}} I_i(x')$, $g_i(x') = e^{-j\beta \frac{x'^2}{2(z-z')}}$ and $I_i(x')$ is an indicator function:

$$I_i(x') = \begin{cases} 1 & x' \in \{\text{Obstacle } i\}\prime \\ 0 & x' \in \{\text{Obstacle } i\}, \end{cases}$$

While we state the preceding results without proof, we refer to [45] for detailed derivations of similar formulas in the context of terrain diffraction where obstacles are treated as knife-edges. Note that the y coordinate perpendicular to the plane of the paper has already been integrated out under the assumption that the obstacle heights extend beyond the first few critical Fresnel zones along the y dimension.

Equation (2) is the convolution of functions $f_i(x) = h_i(x)E_i(x)$ and $g_i(x)$. Successive convolutions as we go from obstacle to obstacle can be efficiently computed using the Fourier transform, since they correspond to multiplications in the frequency domain. In order to obtain accurate field estimates using the FFT and IFFT methods, it is important to choose the spatial sampling intervals such that the aliasing errors are minimized. The size of the computation window should be chosen such that the secondary wave sources outside the computation window do not have a significant effect on the resulting electric field at the receiver. For our example indoor scenarios, we use a computation window of size 2m (400λ) with a 4096 point FFT (sampling interval $< 0.1\lambda$). Also, the minimum gap $(z_{i+1} - z_i)$ between two computation windows i and $i+1$ is assumed to be $\geq$ 25cm for better accuracy of the field predictions that require the distance approximations in the Fresnel-Kirchhoff formulation to hold.

We now show how to modify these computations to account for directivity. Transmit directivity means that the initialization (1) must be modified to account for the transmit antenna array radiation pattern. Referring to Fig. 2, the electric field at a point (z_1, x_1) is given by

$$E_1(x_1) = \frac{E_c}{r_1} e^{-j\beta r_1} A_{tx}(\theta_1(z_1, x_1)), \tag{3}$$

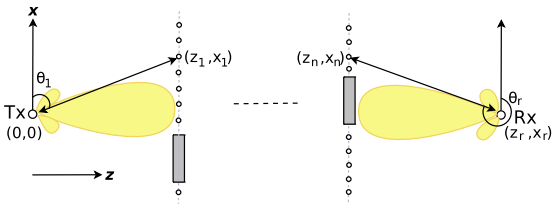

Fig. 2. Effect of directivity on diffraction calculations.

Parameter	Value
Human height range	(1.5m - 2.1m)
RWP model: velocities (min,max), pause time	(0m/s,1m/s), 10s
Fixed obstacle height range	(1m - 1.4m)
WT location height range	(0.5m - 1.5m)
AP location heights home/office	2m/2.5m
Sampling time interval	100ms

TABLE I
INDOOR SETTING PARAMETERS

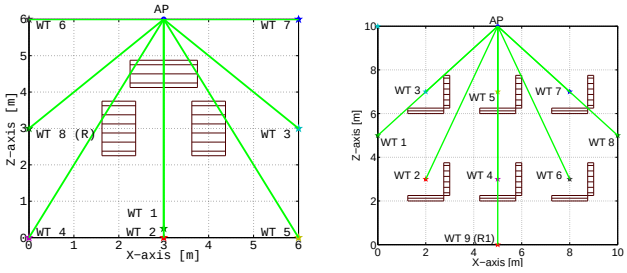

(a) Living room (b) Office

Fig. 3. WPAN simulation scenarios.

where $r_1 = \sqrt{z_1^2 + x_1^2}$, $\frac{E_c}{r_1} e^{-j\beta r_1}$ is the field at (z_1, x_1) due to an isotropic transmit antenna and $A_{tx}(\theta_1(z_1, x_1))$ is the transmit antenna array pattern for an azimuthal angle $\theta_1(z_1, x_1)$ and vertical angle $\phi = 90^o$. The antenna array pattern for different directions can be calculated from the number and placement of antenna array elements, the radiation pattern of elements, and the input array weights [43]. Receive directivity requires the modification of the last step in the computations, as follows: Specifically, the superposition of Huygens' point sources in the plane of the n obstacle at the receiver must account for the receive antenna pattern, as follows:

$$E_{n+1}(x) = \int_{-\infty}^{\infty} h_n(x') E_n(x') A_{rx}(\theta_r(z', x')) g_n(x - x') dx' \quad (4)$$

Here $A_{rx}(\theta_r(z', x'))$ is the receive antenna array field pattern for an azimuthal angle $\theta_r(z', x')$ and vertical angle $\phi = 90^o$. The preceding method accounts for directivity more accurately than the simpler technique [46] that we used in our preliminary results reported in [10], where we calculate the diffraction loss in dB for an isotropic transmission and reception, and add the antenna gains later.

Finally, we express the diffraction loss relative to the free space propagation loss without obstacles. Letting $E = E_{n+1}(x_r)$ denote the field obtained at the receiver, we define the diffraction coefficient $D = \frac{E}{E_{fs}}$, where E_{fs} is the electric field at the same point assuming unobstructed free space propagation. The latter is given by $E_{fs} = \frac{E_c}{d} e^{-j\beta d} A_t A_r$, where E_c is a constant, d is the distance between the transmitter and the receiver, $\beta = \frac{2\pi}{\lambda}$ is the phase constant for wavelength λ, and $A_t = \max_\theta A_{tx}(\theta)$ and $A_r = \max_\theta A_{rx}(\theta)$ are the transmit and receive antenna directivities, respectively, assuming that the transmit and receive antenna arrays are optimally oriented towards each other. The (relative) diffraction loss in dB is given by $L_{dB} = -10 \log_{10} |D|^2$. In order to determine the overall path loss, we simply add it to the unobstructed free space propagation loss in dB.

Indoor Radio Propagation Simulation: Based on the diffraction model described in this section, we have developed a MatLab radio propagation tool to evaluate the link losses between different nodes in a given indoor environment with human beings and other obstacles. This tool yields link losses between different network nodes as a function of time. The inputs to the tool are the parameters required to simulate a WPAN in a specified 3-dimensional indoor environment: the room dimensions; the number, position, and dimensions of the stationary obstacles such as furniture; the number of human beings; the placement of the AP; the number and positions of the WTs; and the antenna configurations. We use the Random Waypoint model [50] for human movements in the room. We assume that all the nodes are equipped with a linear, adaptive beamforming array of 16 isotropic antenna elements spaced $\lambda/2$ apart. The default configuration parameters related to the test scenarios are listed in Table I.

We now use our radio propagation tool to quantify network connectivity for some example WPAN scenarios. We consider two different indoor settings that model typical scenarios where 60 GHz WPANs are expected to be deployed: a living room and an office space (see Figs. 3(a) and 3(b)). The living room scenario has a WPAN formed by an HDTV, a surround sound system with speakers at room corners and a desktop/printer; and has eight human beings, i.e., during a gathering at home. The office space scenario has desktops and printers forming a WPAN, with fifteen human beings. The room and obstacle dimensions and the node placements have been chosen as representative of the real world scenarios in which a large number of people can cause a high blockage probability for the individual links. Note that WT8 in the home scenario and WT9 in the office scenario are placed higher (2.5m) than the other WTs such that they have a high probability of a clear LOS connectivity to most of the WTs and the AP. Hence they can act as effective relays in case the direct LOS connectivity from the AP to a WT is blocked.

We define *connectivity consistency* as the percentage of time out of the total operation period of the network when a WT is reachable from the AP either through a direct LOS link or through a multihop path consisting of live direct links. For illustration, we employ the following link outage criterion for calculation of the expected connectivity consistency: if the diffraction loss due to obstacles exceeds 10 dB for a link, then it is considered to be in outage. This model is pessimistic be-

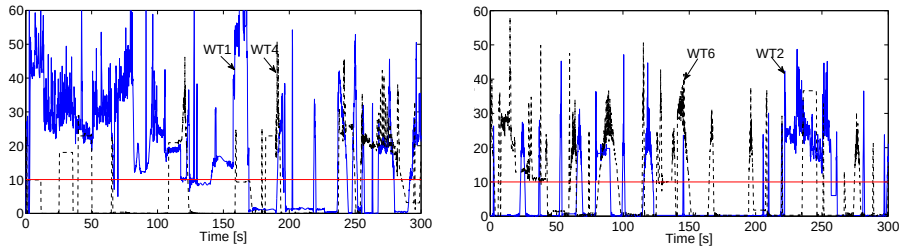

(a) Living room (b) Office

Fig. 4. AP to WT LOS link loss profile.

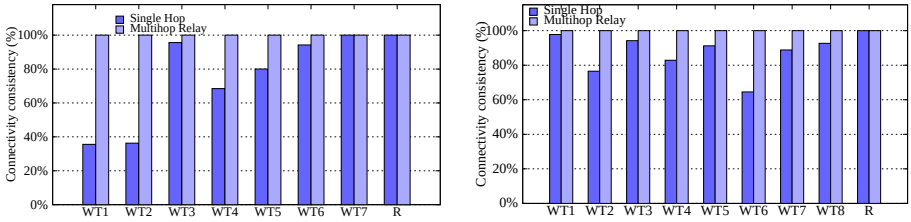

(a) Living room (b) Office

Fig. 5. Connectivity consistency from the AP to different WTs in the single hop baseline and multihop relay MAC (R denotes the primary relay: WT8 in the living room, and WT9 in the office scenario).

cause link budgets are determined based on a maximum range of operation (10 meters for in-room operation). Thus, links over shorter ranges may have enough link margin to "burn through" the obstacles. By abstracting away the dependence of connectivity on range, we obtain a worst-case network connectivity estimate that serves to stress-test the proposed multihop architecture.

We note that connectivity consistency is an indirect metric because the need for connectivity arises only if there is data to transmit at either side. However, considering the importance of an LOS link for maintaining direct connectivity (unlike for 2.4 or 5 GHz WLANs), the links can become blocked easily due to obstacles in indoor environments. Thus, this metric characterizes the actual connection state and the data transfer capacity of the network. This metric can also be interpreted as an indicator of the maximum aggregate throughput sustained by the network when all the nodes have data to send.

Figs. 4(a) and 4(b) plot the variation of the diffraction loss for some specific WT links as a function of time for the living room and office environments over a sample period of 300 seconds. We observe that there are heavy link losses because of the large number of human beings (and their random movements) and the stationary furniture obstacles in both the environments. These obstacles result in intermittent connectivity to the affected WT if the underlying MAC completely relies on the direct single hop connectivity of the AP to the WTs. These loss results demonstrate that networks with the baseline single hop MAC schemes will not be able to provide the required QoS guarantees to different WPAN applications, which are essential requirements for any practical WPAN solution.

Fig. 5 compares the expected connectivity consistency between single hop communication-based approach and a multihop communication scheme that exploits relays to reach the blocked WTs. We observe that, on average, the connectivity consistency for the baseline single-hop communication is significantly lower than the multihop relay scheme, which is able to maintain almost 100% network connectivity by using multihop paths via relay node(s) to connect to the blocked node(s).

Note that the high availability of alternate routes in a multihop architecture can be assured by an appropriate placement of the relay nodes (e.g., high up on the walls, or on the ceiling) accounting for the vertical beamwidths of the WT antennas such that the relays are readily accessible when needed. On the other hand, the poor connectivity consistency of single hop communication makes it unsuitable for WPAN applications with stringent QoS requirements such as multimedia streaming. It is interesting to note that the non-zero single hop connectivity consistency data for both the living room and the office setting implies that no WT is completely blocked by the stationary obstacles. Thus, the moving obstacles (humans) play a key role in causing blockages in both example settings considered. The stationary obstacles constrain human movements and the choice of relays for different WTs because many WTs are blocked from each other.

Having shown that multihop relay helps to maintain consistent connectivity on the face of frequent link blockages due to obstacles, we next present a WPAN MAC protocol that accounts for directional communication and has built-in intelligence for topology discovery and recovery from link blockages via multihop relay.

III. Directional MAC Design

The key idea behind our multihop relay directional MAC framework is to utilize a mix of the conventional AP-based single hop MAC architecture for primary connectivity and

resort to the multihop ad hoc mode with intermediate nodes acting as relays (though still controlled by the AP) to prevent drastic reduction of data rates or link outage when the LOS path to a WT is obstructed. We briefly outline a mechanism for network topology discovery first and then describe the main components of our MAC protocol.

A. Discovery Algorithm

During the network initialization phase, the AP sends a Hello message and waits for the response from the WTs in each sector (the geographical region around a node is divided into equal angular sectors based on the antenna array horizontal beamwidth). The preamble preceding the Hello message payload acts as a training sequence for the WTs to beamform in the AP's direction. The WTs that successfully receive the Hello message record the antenna array weights corresponding to the direction of the AP in their network topology map and use the same weights to respond to the AP, using reciprocity. The unregistered WTs in a sector employ a Slotted Aloha contention scheme for transmitting the Hello Response message over the next m slots following the receipt of the Hello message, with the Hello Response transmission probabilities dictated by the AP (via the Hello and Hello Response ACK messages). Here, a slot duration is sufficient for the transmission of a Hello Response message and the corresponding Hello Response ACK message from the AP to confirm a successful registration. For narrow angular sectors, there is likely to be few WTs in a sector, so the problem of excess collisions is unlikely. After completing a round of discovery with a nominal Hello Response transmit probability (e.g., $0.2 - 0.5$), this procedure can be repeated with a Hello Response transmit probability of one to verify that no WT is left unregistered.

After performing the discovery procedure and having formed a network topology map (i.e, the identities of the WTs in the network and the appropriate antenna array weights required to reach them), the AP iteratively designates each WT among the registered nodes to perform the same discovery procedure. This process continues until all the WTs have finished the discovery procedure and have created their own network topology maps such that each WT is aware of the identities of the other WTs and the appropriate antenna array configurations required to reach them. Every WT sends its network discovery table to the AP after it completes its network discovery process. This information helps the AP deduce the link connectivity status of the whole network, which is useful in the determination of a relay WT when a the direct link to a node is blocked, as described later in this section.

B. Normal Mode of Operation

The AP sequentially polls all the registered WTs to check connectivity to each WT and to check whether any WT has data to transmit. Each WT must respond within a fixed interval, i.e., Poll Inter Frame Space (PIFS), with a data packet or with a *connection live* poll response message if it does not have any data to transmit. This polling-based procedure is required because the conventional carrier sensing medium contention

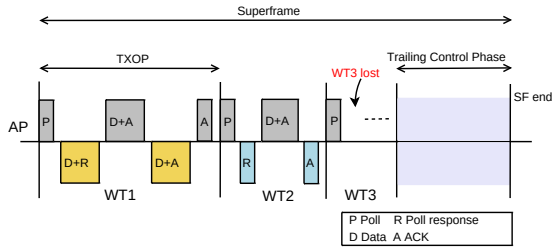

Fig. 6. An example MAC message sequence over a superframe.

schemes do not work well with directional antennas. The polling scheme helps the AP to track the connectivity to all the registered WTs: the absence of a poll response from a WT is assumed to indicate link blockage, and triggers the search for a relay node to set up a multihop relay path to the WT. Note that with a link budget that ensures reliable link operation over the desired range, and in the absence of simultaneous transmissions that can cause interference loss, link blockage from obstacles is the dominant cause of packet loss in this setting. However, interference loss increases when simultaneous transmissions are allowed within the network to achieve high spatial reuse, or in the case of high-density WPAN deployments where multiple networks must coexist in close proximity. The use of a relay node (in addition to other mechanisms such as rate control) can help counter packet loss even in these scenarios. However, additional procedures need to be defined to enable high spatial reuse within a WPAN and coexistence of multiple WPANs. These procedures are topics of future research, and are beyond the scope of this work.

The WT can continue to receive or send data packets until a maximum allowed time duration called the *transmission opportunity* (TXOP) duration. Thus, data transmission in both directions can be bursty because of the sequential transmission of multiple packets in response to the poll message, up to the TXOP duration. Besides providing better QoS performance for the inherently bursty multimedia streaming applications, this allows the WTs to better utilize the available LOS connectivity and also minimizes the control overhead associated with data packet transmissions. If the AP sends a data packet to a WT, the WT acknowledges the successful packet reception either by piggybacking an ACK message on the next data packet that it has for the AP or by sending a separate ACK message.

The AP's dwell time in each sector depends on the data transmission requirements of the WTs in that sector. The AP to WT data transmission mechanism follows a weighted round robin scheduling approach such that the desired level of QoS to different WTs is ensured.

C. Trailing Control Phase

The trailing control phase is utilized by the AP to allow new WTs to register and perform a network discovery procedure while the network is operational. During the trailing control phase, the AP can also verify its own topology map or designate the registered WTs to verify their network topology maps by sequentially sending Hello messages to each WT. The

trailing control phase is limited to a maximum duration, which is larger than the average successful discovery phase time of a node. Because the regular network topology verification procedure of the trailing control phase occurs at a rate much faster than the dynamics of the indoor environments (human movements or change in the room setup), the AP is aware of the LOS connectivity of all the WTs and it can use the topology verification/discovery reports sent back by the WTs to choose a candidate relay node for a blocked WT.

A superframe is defined as the time taken by the AP to poll all the registered WTs in the network. The maximum superframe duration is limited by the number of WTs in the network, the TXOP duration, and the trailing control phase duration. Fig. 6 illustrates an example data transmission and control message sequence over a superframe.

D. Lost Node Discovery and Establishing a Relay Path

If the AP does not receive a poll response from a registered WT, it considers the WT to be *lost* and intelligently chooses a WT among the *live* WTs (with expected LOS connectivity to the lost WT as determined from the regular topology verification reports from the WTs) to act as a relay to the lost node. It commands the chosen relay WT via a Search Lost WT Request message to discover (i.e., check connectivity status with) the lost WT and report back within a stipulated time. The designated relay WT immediately acknowledges the receipt of the Search Lost WT Request message. It then refers to its network topology map information to steer its antenna beam in the direction of the lost WT, and sends a Search message to the lost WT. If the lost WT is able to receive the Search message, it responds with a Search Response message, and infers that it is lost. Note that the packet-by-packet adaptive beamsteering capability (see Section II) enables the lost WT to quickly steer its beam towards the candidate relay WT to receive the Search message and respond back, in case there is no blockage in the direction of the candidate relay WT.

Upon receiving the Search Response message from the lost WT, the chosen relay WT sends a Search Outcome message to the AP, reporting successful lost node discovery and the quality of the link (i.e., the received signal strength) between itself and the lost WT. Otherwise, after waiting for a PIFS interval, the chosen relay WT informs the AP of the lost node discovery failure via the Search Outcome message. Depending on the response from the designated relay WT, the AP decides whether to choose another WT to attempt the lost node discovery procedure or to use the current chosen WT as a relay for the future data transfers to the lost WT. Upon a successful lost WT discovery, the AP adds the required data transfer time for the lost WT to the relay WT's dwell time. The relay WT transparently interfaces the AP and the WT by forwarding the (data/ACK) MAC frames between them based on the destination MAC address of the frames, until the direct link is out of blockage.

The AP continues to send poll messages in the direction of the lost WT over the next superframes, in order to check if the direct link is restored. Once the obstruction is removed and the lost WT starts receiving direct transmissions from the AP, it responds to the AP's poll message. The AP switches back to the normal mode of operation after informing the relay WT to return to its previous state. The dwell times for the directional transmissions to the WTs are adjusted accordingly.

Parameter	Symbol	Value
PHY data rate	R	2 Gbps
Propagation delay	δ_p	50ns
PHY overhead	T_{PHY}	250ns
Header overhead (IP+UDP+MAC)	T_{hdr}	56*8/R
Payload Tx time	$T_{payload}$	1000*8/R
Short MAC frame Tx time	T_{ShFr}	$T_{PHY} + 14 * 8/R + \delta_p$
SIFS interval	T_{SIFS}	100ns
ACK Tx time	T_{ACK}	T_{ShFr}
TXOP duration	T_{TXOP}	100μs
Polling overhead	T_{poll}	$2T_{ShFr} + T_{SIFS}$
Maximum Trailing Control period	T_{TrCP}	50μs
Hello/Hello Response Tx time	T_H/T_{HR}	T_{ShFr}

TABLE II
PROTOCOL PARAMETERS

E. Achievable Rates

In this section, we estimate the aggregate data transfer capacity of our multihop MAC framework. We first find the aggregate throughput for the case when no WT is blocked and packet transmissions to the WTs from the AP are single hop. Then we calculate the change in throughput for the cases when the LOS connectivity to some WTs is lost, and multihop relay is used as an alternative mechanism for data transfer. The underlying goal is to verify that multihop relay results in graceful degradation of overall network throughput rather than loss of connectivity to such WTs altogether, which is extremely undesirable. Given the high data rates afforded by 60 GHz transceiver systems, this reduction in the aggregate throughput does not affect the applications unless the network is operating at full capacity. Also, in order to provide the required quality of service (QoS) support to different WPAN applications, continuous connectivity to all the nodes is essential.

We consider QPSK modulation at 2 Gbps, as in the system described in Section II. We assume that 200 symbols are required for beamformer training and signal acquisition/synchronization, adding 200ns of overhead. While this is adequate for the single carrier system we envision, OFDM might incur additional overhead; the framework for our analysis, however, would remain identical. The physical layer control protocol overhead is assumed to be 50ns. Thus, the total PHY overhead for each data transmission is 250ns. Note that at the nanosecond scale, the propagation delays of signals can no longer be neglected. We assume a maximum propagation delay of 50ns. We also assume that all the nodes operate at the same data rate. The maximum allowed TXOP duration is assumed to be 100μs. The AP polls each registered WT once every superframe and checks connectivity. The superframe duration is allowed to vary as per the data requirements of WTs, but it is limited to a maximum duration (determined by the TXOP interval, the number of WTs, and the system configuration).

We find the maximum aggregate throughput sustained by the network, assuming backlogged UDP flows from the AP to all the WTs with a packet size (P_{size}) of 1000 bytes. This UDP based application model can incorporate the requirements of

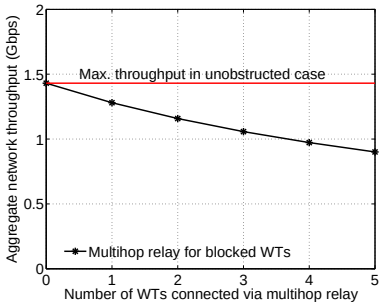

Fig. 7. Aggregate network throughput for an eight WT network as a function of the number of blocked WTs connected via relays.

the common WPAN applications including streaming content download for HDTV, real time streaming and wireless data bus. Table II lists our notation and parameter values.

The total time required to transmit a packet is given by

$$T_{pkt} = T_{PHY} + T_{hdr} + T_{payload} + \delta_p = 4.524\mu s. \quad (5)$$

Every successfully received packet from the AP is acknowledged by an ACK message from the WT since the WTs do not have reverse data traffic. Thus, the total number of packets transmitted in one TXOP is given by

$$N_{pkt} = \frac{T_{TXOP} - T_{poll}}{T_{pkt} + T_{SIFS} + T_{ACK}} = 19. \quad (6)$$

In a network consisting of n active WTs fully utilizing their TXOP duration, the total superframe time will be $T_{SF} = n{\cdot}T_{TXOP} + T_{TrCP}$, which for an eight WT network evaluates to 850μs. We note that this duration is still small enough such that the AP and WTs can closely monitor the changes in network topology and they can adapt to the dynamics of the indoor environment by using multihop relays. Thus, the aggregate throughput S_{SH} sustained by the network under consideration is given by

$$S_{SH} = \frac{n{\cdot}N_{pkt}{\cdot}P_{size}}{T_{SF}}, \quad (7)$$

which equals 1.43 Gbps for the eight WT example. If we assume that m out of n WTs in the network are connected through two hop paths, the T_{SF} increases by mT_{TXOP} to facilitate data transfer over multihop paths without any packet loss. The aggregate throughput S_{MHR} in that case will be

$$S_{MHR} = \frac{n{\cdot}N_{pkt}{\cdot}P_{size}}{T_{SF} + m{\cdot}T_{TXOP}}. \quad (8)$$

Fig. 7 illustrates the aggregate network throughput for an eight WT network as a function of the number of blocked WTs using relays for data transfer. The reduction in aggregate network throughput (as compared with 1.43 Gbps in full single hop connectivity case) is the cost incurred in order to maintain connectivity to all the active WTs and to ensure that even the *lost* WTs do not suffer from packet loss because of blockage of the direct link to the AP. We therefore consider this reduction in the aggregate network throughput as graceful throughput degradation.

We note that at nanoseconds time scales, the packet processing delays at the AP and the WTs are non-negligible and should be accounted for in order to get the actual delays. Because these factors appear in all our time approximations, they will cause a similar shift in the estimates.

IV. Performance Evaluation

A. Simulation Model

We first describe our simulation model which consists of the Matlab radio propagation tool that calculates the link losses (see Section II), and the packet level simulations for performance evaluation of the directional relay MAC protocol. We then present the simulation results and discuss the insights obtained from the results.

Packet Level Network Simulation: We have implemented the multihop relay directional MAC protocol over the QualNet Network Simulator [51]. The link loss data obtained from the Matlab mm-wave propagation tool is fed into the physical layer module of the QualNet simulator, modified to model mm wave communication. The physical layer model also accounts for the antenna directivities while evaluating the signal to interference and noise ratio (SINR) values at each node, which are used to calculate the bit error rates (BER) based on the selected modulation. Packet loss probabilities are evaluated using the BER value and the packet size, which then determine successful or failed packet reception. The MAC and the PHY layer parameters used for the simulations listed in Table II. To obtain the maximum supported data rates in the system, each WT is assumed to download UDP data from the AP such that the AP is always backlogged. The indoor environment is characterized by the parameters listed in Table I. We refer back to the two example scenarios: the living room and the office space (see Figs. 3(a) and 3(b)) introduced in Section II to evaluate the performance of the multihop relay directional MAC protocol.

B. Simulation Results

Fig. 8(a) shows the aggregate network throughput as a function of time for the living room scenario - both for the case with obstacles and in an unobstructed environment. We observe that the aggregate throughput remains fairly consistent, even in the presence of the moving and stationary obstacles. The difference between the two curves quantifies the associated throughput drop (as compared with the throughput achieved in an unobstructed environment) when multihop relay is used to communicate with the blocked WTs that would have otherwise been unreachable from the AP.

The throughput achieved by the individual WTs in the living room setting is shown in Fig. 8(b). All the WTs effectively receive the same average throughput over time because of the equal service weights assigned to all the WTs in the simulations. The assignment of different transmission scheduling weights to packets based on the QoS requirements of the applications at each WT is a trivial extension of the equal weight case presented here. Fig. 8(c) presents the number of WTs connected via multihop paths at different sampling instances of the simulation. We infer that at any time instant, there are a significant number of WTs using multihop relay, which

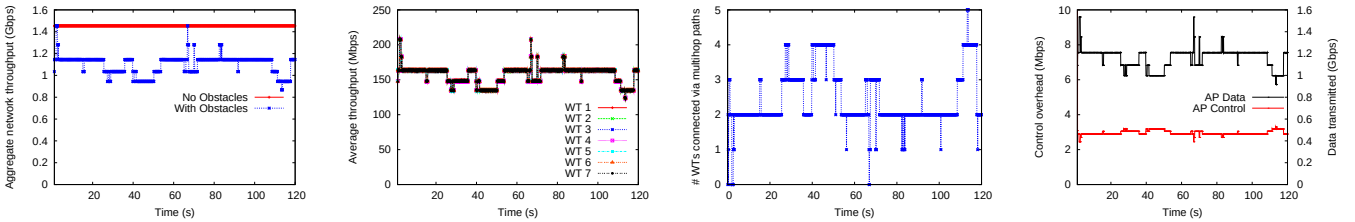

(a) Aggregate network throughput. (b) Individual WT throughputs. (c) Number of WTs connected via multihop paths. (d) AP control overhead and data transmission.

Fig. 8. Protocol performance: living room scenario.

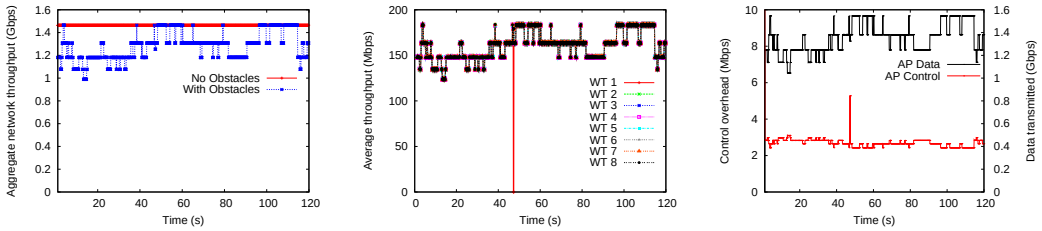

(a) Aggregate network throughput. (b) Individual WT throughputs. (c) AP control overhead and data transmission.

Fig. 9. Protocol performance: office scenario with single relay.

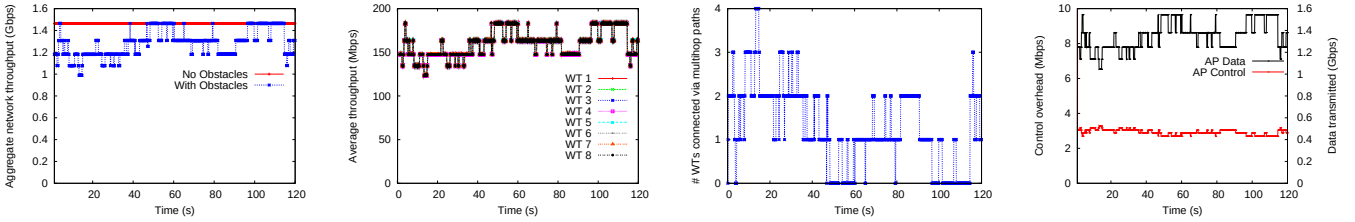

(a) Aggregate network throughput. (b) Individual WT throughputs. (c) Number of WTs connected via multihop paths (d) AP control overhead and data transmission.

Fig. 10. Protocol performance: office scenario with two relays.

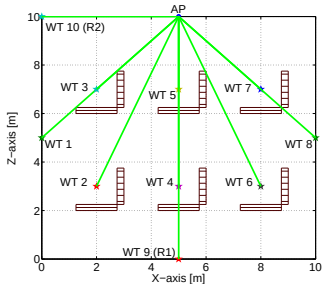

Fig. 11. Office scenario with two relay WTs.

indicates the importance of multihop paths in maintaining uninterrupted network connectivity even under the scenarios where many LOS links are blocked because of obstacles.

Fig. 8(d) illustrates the AP's data transmission rate and the control overhead due to polling, lost node discovery, and relay path setup, as a function of time for the living room scenario. The graph demonstrates the low relative control overhead, and also provides insight into the variation of the control message overhead as a function of the number of WTs on multihop connectivity. The direct relation of the control overhead and the number of nodes on multihop connectivity arises from the lost node discovery and the poll messages for the blocked WTs in each superframe. The AP needs to check whether the WT is back on LOS connectivity in every superframe. Although the AP remembers the corresponding relay WT used in the last superframe to avoid having to search for a relay in every superframe, it needs to check whether the previous relay node is still connected in the current superframe. This accounts for the proportional (although relatively small) increase in the control overhead with increasing number of WTs on multihop paths.

The aggregate network throughput for the office setting is plotted in Fig. 9(a). Fig. 9(b) shows the throughput achieved by the individual WTs. Fig. 9(b) presents an interesting scenario where WT1 is completely inaccessible (i.e., it is blocked from all the other nodes in the network) from 47.0 seconds to 47.3 seconds. Therefore, it achieves zero throughput because the lost node discovery procedure does not yield a relay node for multihop communication to WT1. This example demonstrates that the number and placement of relays play an important role in ensuring that the probability of complete blockage of the

WTs is minimal. Now consider the scenario shown in Fig. 11 where an additional relay node is added to the office network to ensure that no WT is completely isolated. Figs. 10(a) and 10(b) show the aggregate network throughput and the per-WT throughput for this setting, respectively. The additional relay adds redundancy by sharing the relay transmission load and ensures that the network is connected throughout the simulation duration. However, it is important to realize that 100% connectivity consistency cannot be guaranteed for all scenarios - one can imagine different pathological cases where a WT can be completely isolated, although a majority of these scenarios do not correspond to realistic use cases of WPAN devices. Usually the number of required relays depends on how challenging the indoor setting is in terms of the chance of complete blockage of WTs. This likelihood can be minimized by intelligently choosing relay positions (high up on the walls, or on the ceiling) such that they have a better chance of always being connected to the WTs.

Fig. 10(c) shows the number of WTs connected via multihop paths at different sampling instances of the simulation for the office scenario with two relay WTs. The inference is the same as for the living room scenario: multihop relay plays a critical role in maintaining network connectivity and high data rates to each WT.

Figs. 9(c) and 10(d) illustrate the AP's data transmission rate and the associated control overhead as a function of time for the two office scenarios. Fig. 9(c) provides an interesting insight. The spike in the control overhead for the office scenario with a single relay at around 47 seconds is because of the AP's repeated lost node discovery attempts to search for the lost WT1 that is completely isolated for 0.3 seconds. In this example, the AP is configured to continue searching for the lost WT to illustrate the possible high overhead in such cases because of the repeated lost node discovery attempts. This spike can easily be avoided by configuring the AP to search for a lost WT only for a short period of time (equivalently, the AP performs lost node discovery attempts only over a limited number of contiguous superframes), after which the AP should consider the WT to have left the network. The lost WT can join the network again when it comes out of complete blockage (i.e., it can reach one of the network WTs or the AP). Figs. 9(c) and 10(d) also reaffirm the insight on the relationship between the number of nodes on multihop connectivity and the control overhead obtained from the living room scenario.

QoS Performance: Since the multihop directional relay MAC protocol is essentially a contention free transmission scheduling-based MAC protocol, it can offer assured QoS to different applications over the typical WPAN scenarios. Moreover, the protocol can easily be extended to incorporate the well known QoS enhancing MAC features such as block/no acknowledgments and traffic prioritization in IEEE 802.11e HCCA [52]. Since our motivation is to illustrate the promise of multihop relay and directional communication as key enablers for 60 GHz WPANs, we focus on showing their potential via our base protocol.

V. Conclusions and Future Work

Our results illustrate the critical role of cross-layer design in exploiting the large unlicensed bandwidth available in the 60 GHz band. The diffraction-based connectivity model is an effective tool for cross-layer design: it yields results that conform to our intuition that directional LOS mm wave links experience relatively high levels of outage due to stationary and moving obstacles. Despite this fragility of the individual mm wave links, we show via extensive packet-level simulations that the proposed multihop MAC architecture is successful in providing robust connectivity in typical "Superbowl Party" and office settings. Thus, unlike the infrastructure mode operation in the 2.4 GHz and 5 GHz WLANs where the WTs communicate with the AP over a single hop, we believe that multihop communication, possibly with nodes explicitly designated as relays, must play a fundamental role in 60 GHz WPANs.

There are a host of both broad and specific research issues for future research in mm wave WPAN design, of which we mention but a few. An important consideration in cross-layer design is the impact of antenna design and node form factor. We envision the use of circuit board antennas for consumer electronics devices, and the specific integration of such antennas and the mm wave front ends associated with them depends on both form factor and cost constraints. This in turn impacts the coverage of the beams that can be synthesized by these antennas. Thus, while our simulations are for antenna arrays with isotropic elements for simplicity, the physical realization of the network node may impose constraints on network connectivity that must be taken into account. Another important topic for future research is the design of protocols that exploit the significant potential for spatial reuse enabled by the use of highly directional links, and for enabling co-existence of multiple WPANs in close proximity. Another interesting issue is detailed investigation of whether and how reflections can be used to steer around obstacles, as an alternative to, or in combination with, the use of relays. While the point of reflection can be thought of as a virtual relay, we note that the path followed by a reflection is constrained by the geometry of the environment, whereas the placement of an actual relay can be optimized (e.g., it can be put high up on a wall) to maximize connectivity. Much work also remains on detailed physical layer transceiver design for enabling beamsteering with minimal overhead and complexity, which includes cross-layer considerations both from below (RFIC and antenna design) and above (MAC design). Finally, it is important to undertake design and performance evaluation with traffic models aimed specifically at some of the applications driving the interest in high-speed WPANs, such as streaming compressed and uncompressed audio/video, as well as large file transfers.

Acknowledgments

This work was supported in part by the National Science Foundation under grants CNS-0832154, CNS-0520335, CNS-0435527, and Career award CNS-0347886, and by the Institute for Collaborative Biotechnologies under grant DAAD19-03-D-0004 from the US Army Research Office.

REFERENCES

[1] IBMs 60-GHz Page. [Online]. Available: http://domino.research.ibm.com/comm/research_projects.nsf/pages/mmwave.sixtygig.html

[2] 60 GHz CMOS Radio Design at Berkeley Wireless Research Center. [Online]. Available: http://bwrc.eecs.berkeley.edu/Research/OGRE/index.htm

[3] WIGWAM - Wireless Gigabit with Advanced Multimedia Support. [Online]. Available: http://www.wigwam-project.de/

[4] NICTA - Wireless GigE. [Online]. Available: http://www.nicta.com.au/research/projects/60ghz_wireless

[5] N. Guo, R. C. Qiu, S. S. Mo, and K. Takahashi, "60-GHz Millimeter-Wave Radio: Principle, Technology, and New Results," *EURASIP J. Wirel. Commun. Netw.*, vol. 2007, no. 1, pp. 48–48, 2007.

[6] S. K. Yong and C.-C. Chong, "An overview of multigigabit wireless through millimeter wave technology: potentials and technical challenges," *EURASIP J. Wirel. Commun. Netw.*, vol. 2007, no. 1, pp. 1–10, 2007.

[7] IEEE 802.15 WPAN Millimeter Wave Alternative PHY Task Group 3c (TG3c). [Online]. Available: http://www.ieee802.org/15/pub/TG3c.html

[8] WirelessHD. [Online]. Available: http://wirelesshd.org/

[9] ECMA International. [Online]. Available: http://www.ecma-international.org/

[10] S. Singh, F. Ziliotto, U. Madhow, E. Belding, and M. Rodwell, "Millimeter wave WPAN: Cross-layer modeling and multi-hop architecture," *Proc. IEEE INFOCOM 2007*, pp. 2336–2340, 6-12 May 2007.

[11] R. R. Choudhury, X. Yang, R. Ramanathan, and N. H. Vaidya, "On designing mac protocols for wireless networks using directional antennas," *IEEE Trans. Mob. Comput.*, vol. 5, no. 5, pp. 477–491, 2006.

[12] R. Ramanathan, J. Redi, C. Santivanez, D. Wiggins, and S. Polit, "Ad hoc networking with directional antennas: a complete system solution," *IEEE J. Sel. Areas Commun.*, vol. 23, no. 3, pp. 496–506, March 2005.

[13] T. Korakis, G. Jakllari, and L. Tassiulas, "CDR-MAC: A protocol for full exploitation of directional antennas in ad hoc wireless networks," *IEEE Trans. Mob. Comput.*, vol. 7, no. 2, pp. 145–155, Feb. 2008.

[14] A. Nasipuri, S. Ye, J. You, and R. Hiromoto, "A mac protocol for mobile ad hoc networks using directional antennas," *Proc. IEEE WCNC 2000*, vol. 3, pp. 1214–1219 vol.3, 2000.

[15] M. Takai, J. Martin, R. Bagrodia, and A. Ren, "Directional virtual carrier sensing for directional antennas in mobile ad hoc networks," in *Proc. ACM MobiHoc 2002*. New York, NY, USA: ACM, 2002, pp. 183–193.

[16] R. R. Choudhury and N. H. Vaidya, "Deafness: A mac problem in ad hoc networks when using directional antennas," *Proc. IEEE ICNP 2004*, pp. 283–292, 2004.

[17] H. Singh and S. Singh, "Smart-aloha for multi-hop wireless networks," *Mob. Netw. Appl.*, vol. 10, no. 5, pp. 651–662, 2005.

[18] G. Jakllari, W. Luo, and S. V. Krishnamurthy, "An integrated neighbor discovery and mac protocol for ad hoc networks using directional antennas," in *Proc. IEEE WOWMOM 2005*. Washington, DC, USA: IEEE Computer Society, 2005, pp. 11–21.

[19] SiBEAM. [Online]. Available: http://www.sibeam.com/

[20] H. Xu, V. Kukshya, and T. S. Rappaport, "Spatial and Temporal Characteristics of 60 GHz Indoor Channels," *IEEE J. Sel. Areas Commun.*, vol. 20, no. 3, pp. 620–630, Apr. 2002.

[21] N. Moraitis and P. Constantinou, "Indoor Channel Measurements and Characterization at 60 GHz for Wireless Local Area Network Applications," *IEEE Trans. Antennas Propag.*, vol. 52, no. 12, pp. 3180–3189, Dec. 2004.

[22] P. F. M. Smulders, "Broadband Wireless LANs: A Feasibility Study," Ph.D. dissertation, Eindhoven University of Technology, The Netherlands, 1995.

[23] T. Manabe, K. Sato, H. Masuzawa, K. Taira, T. Ihara, Y. Kasashima, and K. Yamaki, "Effects of Antenna Directivity and Polarization on Indoor Multipath Propagation Characteristics at 60 GHz," *IEEE J. Sel. Areas Commun.*, vol. 14, no. 3, pp. 441–448, Apr. 1996.

[24] H. Yang, M. Herben, and P. Smulders, "Impact of Antenna Pattern and Reflective Environment on 60 GHz Indoor Radio Channel Characteristics," *IEEE Antennas Wireless Propagat. Lett.*, vol. 4, pp. 300–303, Jun. 2005.

[25] J. Kunisch, E. Zollinger, J. Pamp, and A. Winkelmann, "MEDIAN 60GHz Wideband Indoor Radio Channel Measurements and Model," in *Proc. IEEE VTC 1999*, Amsterdam, The Netherlands, Sep. 1999.

[26] T. Zwick, T. J. Beukema, and H. Nam, "Wideband channel sounder with measurements and model for the 60 GHz indoor radio channel," *IEEE Trans. on Veh. Tech.*, vol. 54, no. 4, pp. 1266–1277, July 2005.

[27] M.-S. Choi, G. Grosskopf, and D. Rohde, "Statistical characteristics of 60 GHz wideband indoor propagation channel," *Proc. IEEE PIMRC 2005*, vol. 1, pp. 599–603, Sept. 2005.

[28] C. Anderson and T. Rappaport, "In-building wideband partition loss measurements at 2.5 and 60 GHz," *IEEE Tran. Wireless Commun.*, vol. 3, no. 3, pp. 922–928, May 2004.

[29] A. Hammoudeh, D. Scammell, and M. Sanchez, "Measurements and analysis of the indoor wideband millimeter wave wireless radio channel and frequency diversity characterization," *IEEE Trans. Antennas Propagat.*, vol. 51, no. 10, pp. 2974–2986, Oct. 2003.

[30] P. F. M. Smulders, "Deterministic Modelling of Indoor Radio Propagation at 40 – 60 GHz," *Wireless Pers. Commun.*, vol. 1, no. 2, pp. 127–135, Jun. 1994.

[31] F. Villanese, N. E. Evans, and W. G. Scanlon, "Pedestrian-Induced Fading for Indoor Channels at 2.45, 5.7 and 62GHz," in *Proc. IEEE VTC 2000*, Boston, MA, Sep. 2000.

[32] M. Williamson, G. E. Athanasiadou, and A. R. Nix, "Investigating the Effects of Antenna Directivity on Wireless Indoor Communication at 60GHz," in *Proc. IEEE PIMRC'97*, Helsinki, Finland, Sep. 1997.

[33] T. Manabe, K. Sato, H. Masuzawa, K. Taira, T. Ihara, Y. Kasashima, and K. Yamaki, "Polarization Dependence of Multipath Propagation and High-speed Transmission Characteristics of Indoor Millimeter-Wave Channel at 60 GHz," *IEEE Trans. Veh. Technol.*, vol. 44, no. 2, pp. 268–274, May 1995.

[34] P. F. M. Smulders, "Exploiting the 60 GHz Band for Local Wireless Multimedia Access: Prospects and Future Directions," *IEEE Commun. Mag.*, vol. 40, no. 1, pp. 140–147, Jan. 2002.

[35] S. Collonge, G. Zaharia, and G. Zein, "Influence of the human activity on wide-band characteristics of the 60 GHz indoor radio channel," *IEEE Tran. Wireless Commun.*, vol. 3, no. 6, pp. 2396–2406, Nov. 2004.

[36] K. Sato and T. Manabe, "Estimation of Propagation-Path Visibility for Indoor Wireless LAN Systems under Shadowing Condition by Human Bodies," in *Proc. IEEE VTC 1998*, Ottawa, Canada, May 1998.

[37] R. Janaswamy, "An Indoor Pathloss Model at 60 GHz Based on Transport Theory," *IEEE Antennas Wireless Propagat. Lett.*, vol. 5, pp. 58–60, 2006.

[38] S.-K. Yong, "Tg3c channel modeling sub-committee report," IEEE 802.15 WPAN Millimeter Wave Alternative PHY Task Group 3c (TG3c), Tech. Rep. IEEE 15-07-0584-01-003c, Mar. 2007.

[39] J. D. Kraus, *Antennas for all Applications.* NY: McGraw-Hill, Inc., 2002.

[40] U. Madhow, *Fundamentals of Digital Communication*. New York, NY: Cambridge University Press, 2008.

[41] S. Bellofiore, J. Foutz, C. Balanis, and A. Spanias, "Smart-antenna system for mobile communication networks. part 2. beamforming and network throughput," *IEEE Antennas and Propagat. Mag.*, vol. 44, no. 4, pp. 106–114, Aug 2002.

[42] A. Sayed, *Fundamentals of Adaptive Filtering*. IEEE Press, 2003.

[43] S. J. Orfanidis, *Electromagnetic Waves and Antennas.* Piscataway, NJ: Online Book., Feb. 2008. [Online]. Available: http://www.ece.rutgers.edu/~orfanidi/ewa/

[44] J. D. Kraus, *Electromagnetics*. NY: McGraw-Hill, Inc., 1991.

[45] J. H. Whitteker, "Fresnel-Kirchhoff theory applied to terrain diffraction problems," *Radio Science*, vol. 25, pp. 837–851, Oct. 1990.

[46] J. Whitteker, "Physical Optics and Field-strength Predictions for Wireless Systems," *IEEE J. Sel. Areas Commun.*, vol. 20, no. 3, pp. 515–522, Apr 2002.

[47] T. S. Rappaport, *Wireless Communications: Principles and Practice*. Upper Saddle River, NJ: Prentice Hall, Inc., 2002.

[48] J. D. Parsons, *The Mobile Radio Propagation Channel*. New York: John Wiley and Sons, Ltd., 2000.

[49] T. Russell, C. Bostian, and T. Rappaport, "A deterministic approach to predicting microwave diffraction by buildings for microcellular systems," *IEEE Trans. Antennas Propagat.*, vol. 41, no. 12, pp. 1640–1649, Dec 1993.

[50] C. Bettstetter, H. Hartenstein, and X. Pérez-Costa, "Stochastic Properties of the Random Waypoint Mobility Model," *Wirel. Netw.*, vol. 10, no. 5, pp. 555–567, 2004.

[51] Qualnet Network Simulator, version 4.1. [Online]. Available: http://www.scalable-networks.com

[52] "Wireless LAN Medium Access Control (MAC) and Physical Layer (PHY) specifications Amendment 8: Medium Access Control (MAC) Quality of Service Enhancements," IEEE Std. 802.11e-2005, Nov. 2005.

Sumit Singh received the bachelors degree in Electrical Engineering from the Indian Institute of Technology, Bombay, in 2002. He worked as a software engineer in the Network Systems Division at Samsung Electronics, Bangalore from 2002 to 2004. Sumit is currently pursuing the Ph.D. degree in Electrical and Computer Engineering at the University of California, Santa Barbara, where he is working with Prof. Upamanyu Madhow and Prof. Elizabeth M. Belding. His research interests lie in wireless networking, particularly medium access control, resource allocation, and quality of service in wireless networks.

Federico Ziliotto obtained the "Laurea" (Msc) degree in Telecommunications Engineering from the University of Padova, Italy, in 2006. He wrote his graduation thesis "System Blockage Model for WPANs in the 60 GHz Band" as the result of a scholarship period in the research group of Prof. Upamanyu Madhow, at the University of California, Santa Barbara. Right after the university, Federico worked first as a customer support engineer for Infovista in Paris, France. In April 2007 he moved to Brussels, Belgium, where he is currently employed as a customer support engineer in wireless, AAA, identity based networks and network access control technologies for Cisco Systems. In January 2009 Federico obtained the CCIE Wireless certification #23280.

Upamanyu Madhow received his bachelor's degree in electrical engineering from the Indian Institute of Technology, Kanpur, in 1985. He received the M. S. and Ph. D. degrees in electrical engineering from the University of Illinois, Urbana-Champaign in 1987 and 1990, respectively.

From 1990 to 1991, he was a Visiting Assistant Professor at the University of Illinois. From 1991 to 1994, he was a research scientist at Bell Communications Research, Morristown, NJ. From 1994 to 1999, he was on the faculty of the Department of Electrical and Computer Engineering at the University of Illinois, Urbana-Champaign. Since December 1999, he has been with the Department of Electrical and Computer Engineering at the University of California, Santa Barbara, where he is currently a Professor. His research interests are in communication systems and networking, with current emphasis on wireless communication, sensor networks and multimedia security.

Dr. Madhow is a recipient of the NSF CAREER award. He has served as Associate Editor for the IEEE Transactions on Communications, IEEE Transactions on Information Theory, and IEEE Transactions on Information Forensics and Security. He is the author of the graduate textbook, Fundamentals of Digital Communication, published by Cambridge University Press.

Elizabeth M. Belding is a Professor in the Department of Computer Science at the University of California, Santa Barbara. Elizabeth's research focuses on mobile networking, specifically mesh networks, multimedia, monitoring, and solutions for networking in under-developed regions. She is the founder of the Mobility Management and Networking (MOMENT) Laboratory (http://moment.cs.ucsb.edu) at UCSB. Elizabeth is the author of over 80 papers related to mobile networking and has served on over 50 program committees for networking conferences. Elizabeth served as the TPC Co-Chair of ACM MobiCom 2005 and IEEE SECON 2005, and the TPC Co-Chair of ACM MobiHoc 2007. She also served on the editorial board for the IEEE Transactions on Mobile Computing. Elizabeth is the recipient of an NSF CAREER award, and a 2002 Technology Review 100 award, awarded to the world's top young investigators. See http://www.cs.ucsb.edu/ ebelding for further details.

Mark Rodwell (B.S., University of Tennessee, Knoxville, 1980, M.S. Stanford University 1982, Ph.D. Stanford University 1988) is Professor and Director of the UCSB Nanofabrication Laboratory and NSF Nanofabrication Infrastructure Network (NNIN), and the SRC Nonclassical CMOS Research Center at the University of California, Santa Barbara. He was at AT&T Bell Laboratories, Whippany, N.J. during 1982-1984. His research focuses on very high frequency transistors and integrated circuits. Current efforts include THz InP bipolar transistors, compound semiconductor field-effect-transistors for VLSI applications, and mm-wave and sub-mm-wave integrated circuit design in both silicon VLSI and III-V processes. He was the recipient of a 1989 National Science Foundation Presidential Young Investigator award, his work on GaAs Schottky-diode ICs for mm-wave instrumentation was awarded the 1997 IEEE Microwave Prize, and he was elected IEEE Fellow in 2003.